Reports

Lunar Apennine-Hadley Region: Geological Implications of Earth-Based Radar and Infrared Measurements

Abstract. *Recently completed high-resolution radar maps of the moon contain information on the decimeter-scale structure of the surface. When this information is combined with eclipse thermal-enhancement data and with high-resolution Lunar Orbiter photography, the surface morphology is revealed in some detail. A geological history for certain features and subareas can be developed, which provides one possible framework for the interpretation of the findings from the Apollo 15 landing. Frequency of decimeter- and meter-size blocks in and around lunar craters, given by the remote-sensed data, supports a multilayer structure in the Palus Putredinis mare region, as well as a great age for the bordering Apennine Mountains scarp.*

The reflectivity of the lunar surface in the visible and at radar wavelengths and its infrared emission is different from place to place. The observed variations have prompted a series of studies to correlate the findings and relate them to the surface geology (*1*). In this report, attention is focused on the Apennine-Hadley region which includes the Apollo 15 landing site.

The two radar studies used in this work are similar except for the wavelength. The maps at 70-cm wavelength (*2*) have a 5- to 10-km surface resolution for the inner 70° of the earthside lunar hemisphere. The recent maps at 3.8 cm (*3*) have a 2- to 3-km resolution for the entire earthside lunar hemisphere. The observations utilized circularly polarized radiation with both the "polarized" and "depolarized" backscattered radiation being mapped (*4*). The depolarized measurements will be emphasized, since they are significantly less affected by local surface slopes and thus give a more accurate representation of the lunar surface itself.

A number of theoretical treatments have been made of the reflection of radar waves from the lunar surface (*3*, *5*). In general, local enhancement in the radar backscatter will result from increases in the dielectric constant, the roughness on the scale of the wavelength, or the slope of the surface. Measurements of the electrical conductivity of lunar samples (*6*) confirm that the radar echoes can be expected from depths of about ten wavelengths with an attenuation of no more than 0.1.

The infrared brightness temperature of the moon's surface was observed during a lunar eclipse (*7*). Scans of the disk at 15-km resolution revealed the presence of hundreds of small thermal anomalies, which have been identified with a variety of geological features. In addition, some mare surfaces are thermally anomalous. Whereas the average lunar surface cools about 200°K during the first hour of an eclipse and then about 20°K more during total eclipse, the anomalous areas are found to cool more slowly and to maintain a temperature difference of a few degrees to more than 100°K above the average surface. These elevated temperatures have been explained by the large thermal inertia of bare surface rocks (*8*). Winter (*9*) has shown from Surveyor data that an anomalous number of surface rocks that are 10 cm or larger can explain the observed anomalous thermal behavior.

We have examined the radar and infrared observations for the Apennine-Hadley region, in particular the area 20° to 28°N and 0° to 8°E (see Fig. 1A). In this area, the most prominent feature is the scarp of the Apennine Mountains. To the northwest of the crest of the mountains is an approximately level plain broken only by isolated hills and northeast-trending ridges, which are probably elevated portions of the Imbrium Basin floor. The level terrain is formed mainly by two post-basin units, the older Apennine Bench Formation (*10*) and the younger mare material of Palus Putredinis, which is seen to obliterate features of the Apennine Bench. On the other side of the scarp a series of segmented, generally rectilinear massifs such as Mount Hadley form the crest of the Apennine Mountains. Southeast of the crest line, the terrain is rough at the 1-km scale and slopes gently off to the southeast.

From their location, the Apennine Mountains are almost certainly a product of the event that formed the Imbrium Basin, at a time substantially later than several of the other nearby major basins such as Serenitatis and Vaporum. If the formation of these earlier basins distributed lunar material over the area now occupied by Mare Imbrium, which is highly likely in view of the energies involved, then the faulting, tilting, or overturning that resulted in the present appearance of the Apennine Mountains has probably exposed a sequence of such layers. Such a distribution of physical strata would not only influence the appearance of this area in our earth-based mappings but should, through observation or sampling by the Apollo astronauts, provide information on a generous part of lunar geologic history.

To simplify the discussion, we have divided the area into three major, morphologically distinct units: the Apennine Crest, the Apennine Backslope, and Palus Putredinis.

Apennine Crest. The Apennine Crest shows a series of very bright radar returns at 3.8 and 70 cm that coincide with the earth-facing slopes of the major mountain peaks. The 3.8-cm polarized returns are in some cases 40 times greater than the average return, with corresponding depolarized returns of more than 10 times the average (Fig. 1, B and C).

We may separate the effect of the slope from the inherent reflectivity of the surface by examining the data in both the polarized and depolarized radar maps, for both the earth-facing side and the opposite side of Mount Hadley. Predicted values for the radar echoes were calculated with the use of the mean lunar 3.8-cm radar scattering law (*3*) on the assumption of a range of surface slopes from 15° to 30° and an otherwise average surface. The result is a set of values from 1/7 to 1/2 of the observed echoes. If this discrepancy is attributed entirely to the dielectric constant of the surface, an increase in the dielectric constant is required from the nominal $\varepsilon = 2.7$ to $\varepsilon \geqq 5$, which approaches solid rock (*6*). This interpretation is not consistent with the infrared measurements, which show an average response for the Mount Hadley region rather than the strong enhancement that such a rock surface would produce. Nor is it consistent with the high-resolution Orbiter photographs, which show on the steep mountain slopes a series of horizontal ripple marks typical of flow patterns for loosely compacted soil material.

Alternatively, if the discrepancy in echo strength were a result of an increase in the roughness of the surface, the depolarized echo from the slope facing away from the earth would be stronger than average, whereas measurements showed that it was weaker ($0.6 \times$ average).

One reasonable interpretation of the measurements is a smooth and dense surface, with a dielectric constant in the neighborhood of 4.0 and with no more than an average number of surface and near-surface rocks in the size range larger than 1 cm. This block-poor condition suggests a great age for the mountains, as well as confirming the thick regolith layer underlying Palus Putredinis (see below).

Apennine Backslope. The Apennine Backslope area contains two strips generally parallel to the ridge with different appearances on the radar maps but not on the infrared. The strip within 100 km of the ridge shows a moderately enhanced response at both 3.8- and 70-cm radar wavelengths and an average response in the infrared, in agreement with its optical appearance as a typical highland region. Beyond this strip, about 100 km to the southeast of the ridge, lies a region of lower radar response (0.7 times the average at 3.8 cm and average at 70 cm), but with an unchanged average response in the infrared. The regolith in this region appears more fine-grained here than it does nearer the ridge and contains only an average number of rocks in the centimeter to meter range with few rocks exposed at the surface. This condition may be the result of a more recent surface deposit of fine-grained material. This interpretation is supported by the

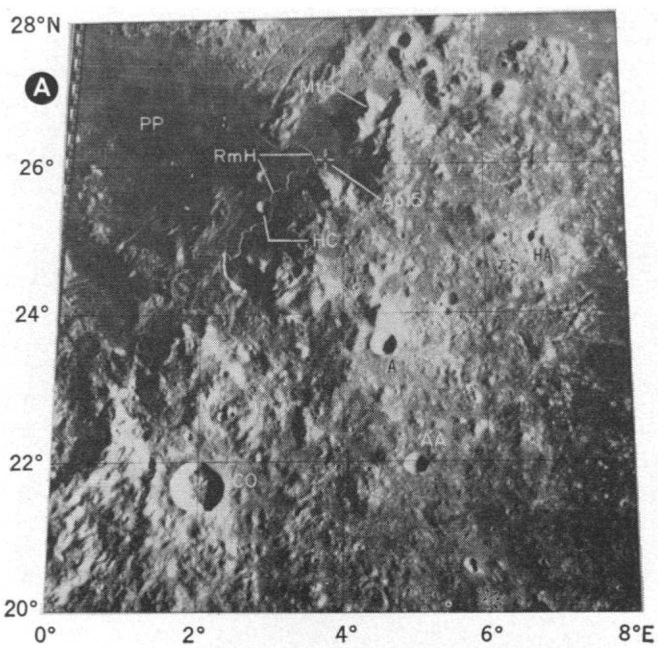

Fig. 1. (A) Lunar Orbiter photography of the Apennine-Hadley region (Lunar Orbiter 4, frame 102-H3). The following craters are designated: *A*, Aratus; *HC*, Hadley C; *CO*, Conon; *HA*, Hadley A; and *AA*, Aratus A. Other features are: *RmH*, Rima Hadley; *Ap15*, Apollo 15 landing target; *MtH*, Mount Hadley; and *PP*, Palus Putredinis. (B) Polarized (*4*) 3.8-cm wavelength radar backscatter map. The apparent shadowing and topographic relief, which is an artificial result of the slope angle-dependence of the radar echo strength, helps in the identification of radar features on optical maps. (Resolution, approximately 2 km.) (C) Depolarized (*4*) 3.8-cm wavelength radar backscatter map. Bright features possess an excess of near-surface blocks in the size range of 1 to 20 cm; or possibly a large increase above the average dielectric constant for the surface. Surface slope angle has little apparent effect on the echo strength. Feature identification can be carried over from Fig. 1B, since the coincidence of the two radar maps is exact. (Resolution, approximately 2 km.)

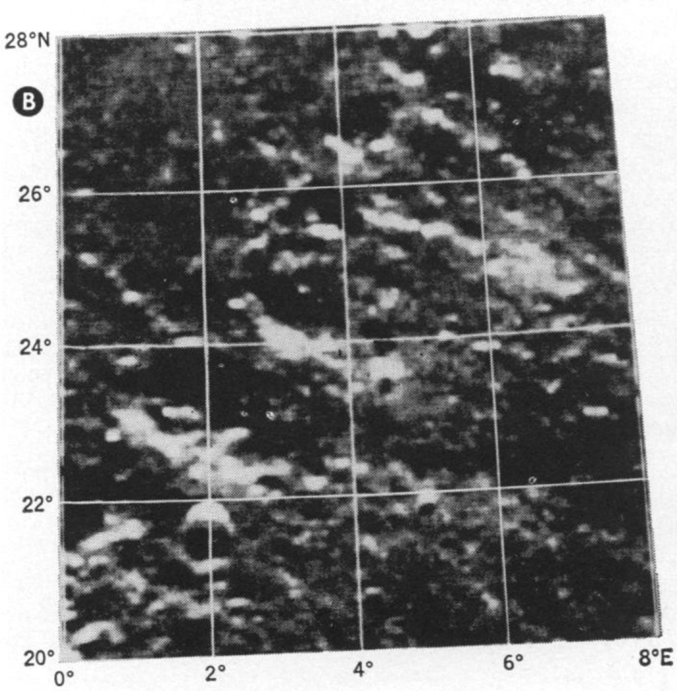

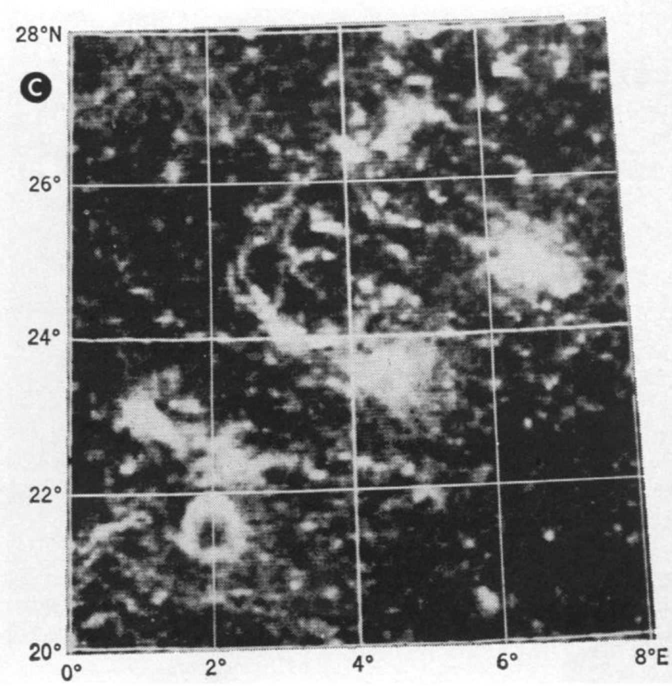

3.8-cm radar appearance of small craters, where the contrast with similar craters on Palus Putredinis is discussed below.

Palus Putredinis. In Palus Putredinis the radar albedo may be locally enhanced by as much as a factor of 3. A number of bright, diffuse radar patches prove to be small (<1 km) craters, surrounded by a radar halo that may extend up to ten crater diameters from the center. Occasionally, such a radar patch has no obvious optical counterpart (see Fig. 1C at 26.7°N, 1.6°E). This is in contrast to the Apennine Backslope, where radar halos around small craters have sharper boundaries and generally extend no more than three crater diameters. The differences in radar response indicate a different block-size frequency distribution for the two regions: craters in the Apennine Backslope will have fewer radar wavelength-size blocks at distances out to three to ten crater diameters than will craters of similar size in the mare. There are two possible explanations for this result: (i) fewer blocks were formed by the cratering event because of the poorly cohesive nature of the original substrate; and (ii) the blocks so formed were more friable in this region and hence were more easily eroded away. This interpretation is supported by the friable nature of some of the Apollo 14 rocks (*11*).

Most of the southeastern part of Palus Putredinis has a very low radar albedo. North of 27°N, however, the mare surface of Palus Putredinis is enhanced in the 3.8-cm radar (and possibly in the infrared) compared with the mare farther south. The dividing line between the two albedo regions is very sharp but does not appear to coincide with any topographic or optically detectable feature. Different flows may be

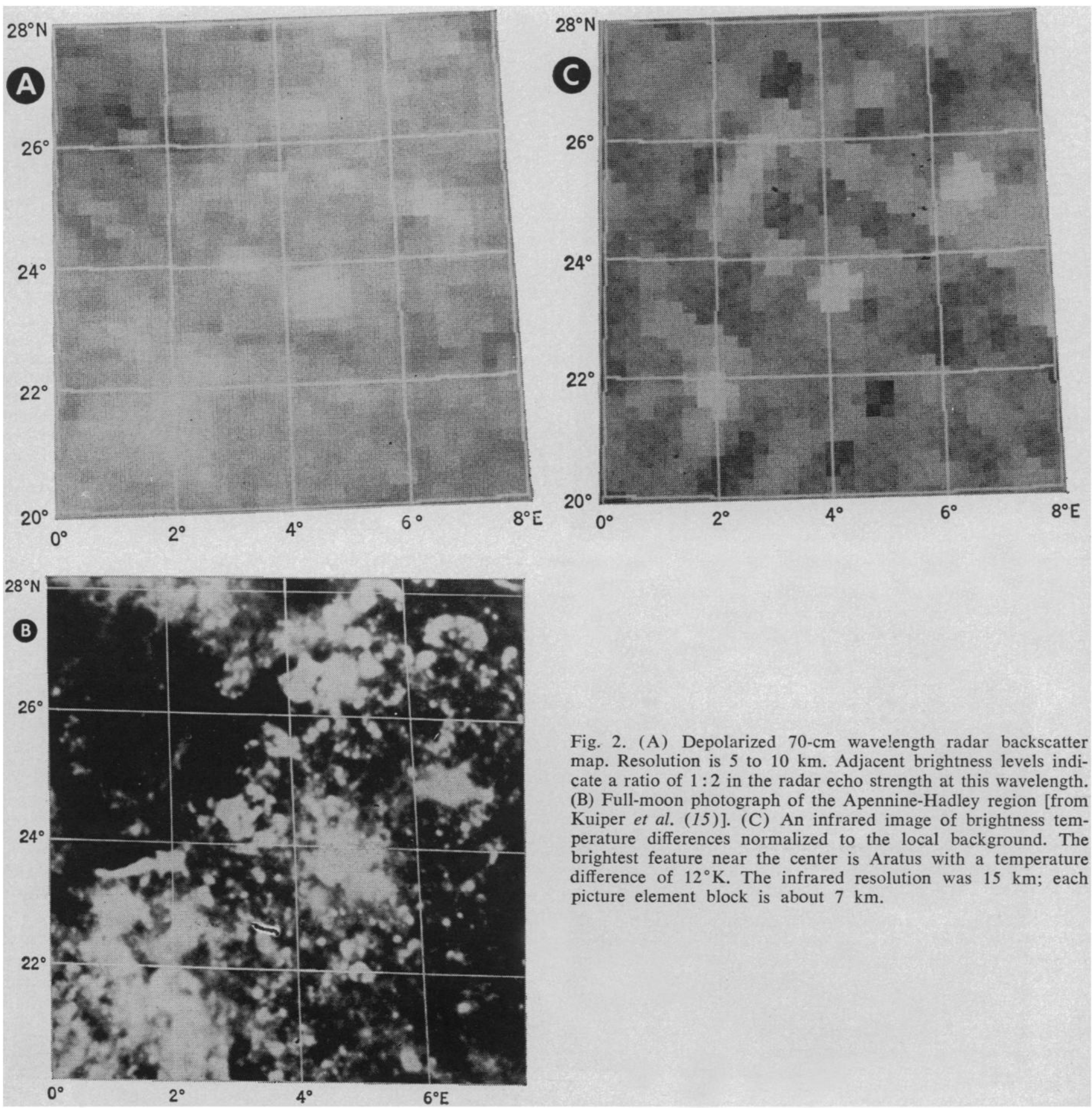

Fig. 2. (A) Depolarized 70-cm wavelength radar backscatter map. Resolution is 5 to 10 km. Adjacent brightness levels indicate a ratio of 1:2 in the radar echo strength at this wavelength. (B) Full-moon photograph of the Apennine-Hadley region [from Kuiper *et al.* (*15*)]. (C) An infrared image of brightness temperature differences normalized to the local background. The brightest feature near the center is Aratus with a temperature difference of 12°K. The infrared resolution was 15 km; each picture element block is about 7 km.

indicated or maria of different ages, the more blocky and presumably older mare being in the north. Another possibility is that the mare in the south is covered with a thin layer of fine debris of low radar albedo and of optical albedo as low as the rest of the mare. The presence of such material is suggested by the low optical albedo of some adjacent ridges and hills, features that normally have a much higher albedo. They are visible on the radar maps because of the enhancing effect of their slopes. A less likely explanation is that the radar enhancement in the north indicates a layer of Aristillus/Autolycus ray material, but the sharp boundary between the regions argues against this.

Small-scale features. Rima Hadley on the 3.8-cm radar map is a thin, somewhat broken line, while both infrared and 70-cm radar (Fig. 2, A and C) show an extended enhancement whose width is undoubtedly due to the more limited resolution (*12*). The deep cleft at its southern end is a strong radar scatterer, which indicates a near-surface texture that is moderately blocky. The rille itself, however, is not nearly so bright as, for example, Rima Hyginus. The crater chains in Hyginus strongly favor a volcano-tectonic origin, and the marked 3.8-cm radar and infrared enhancements suggest abundant blocky debris, with mostly decimeter sizes in view of the moderate (2 : 1) 70-cm radar enhancement. The weaker radar return for Hadley can be interpreted as supporting a different origin. The hypothetical lava tube (*13*) might well result in a weaker radar return for Hadley since the only sources of blocks are the walls of the tube, rather than the several volcanic pipes, as is possibly the case with Hyginus.

At Hadley C (25.5°N, 2.8°E), its ejecta appears to fill part of the Hadley Rille (Fig. 1A) indicating a younger age for the crater than for the rille. The sharp bottom and smooth conical profile of the crater walls also indicate that the crater is quite young. Unlike the typical young crater, however, it shows very little infrared enhancement or enhanced 3.8- or 70-cm radar backscatter; in fact, it is difficult to distinguish on the radar map. It appears to be relatively free of smaller rocks, therefore, despite its 5-km diameter and 0.8-km depth. From Orbiter photographs even the larger blocks appear to be missing, and full-moon photographs (Fig. 2B) also show no brightness.

Several mechanisms could explain the block deficiency. The mare rock layer may be so thin here that the crater is formed largely in underlying, less cohesive materials, which yielded fewer blocks during the original event than would appear on a more typical mare. Alternatively, the crater may be volcanic, resulting in deposition of only fine-grained debris. Since blocks disappear with time (*14*), the lack of blocks may, in spite of the morphology, be due to a relatively old age for the crater. Other features of the crater do suggest an Eratosthenian age, by which time most large, photographically evidenced blocks would typically have disappeared from the surface. However, the absence of any radar enhancement suggests few decimeter- and meter-size blocks are present even to a depth of several meters. This is difficult to explain on the basis of aging alone, and argues for a more unusual geology for the crater.

There are three outstanding examples of large radar and infrared crater enhancements located within this region: the craters Aratus (24.7°N, 4.6°E), Hadley A (21.8°N, 1.9°E), and Conon (21.8°N, 1.9°E). Of the three, Aratus and Hadley A are extremely enhanced in the 3.8- and 70-cm radar and in infrared, are bright in full-moon photographs, and also appear fresh, blocky, and sharp in the high-resolution Lunar Orbiter photographs. There appears, therefore, to be an extensive field of decimeter- and meter-size rocks surrounding these craters and extending out to about 10 km from each of these craters. These features suggest that Aratus and Hadley A are very young (Copernican).

Conon is quite bright on the 70-cm radar map but only moderately enhanced on the infrared map. On the 3.8-cm map, as well as the full-moon photographs, the rim is quite bright, but there is only a slight enhancement of the floor and surroundings. Conon appears, therefore, to be an older (Eratosthenian) crater, in which the original population of surface rocks has been depleted everywhere except on the rim but an excess of meter-size rocks remains a few meters below the surface. Such rim-bright craters are relatively common. They may develop because the rocks buried in the crater walls are exposed by the normal processes of erosion, and the finer-grained erosion products are then deposited on the lower ground both surrounding and within the walls, thereby reducing still further the radar reflectivity of these areas.

An interesting contrast in crater ages can be drawn by examination of Aratus A (22.0°N, 5.0°E), in comparison with the similar-sized blocky crater Aratus. Aratus A shows the flat-bottomed, rounded floor and smooth walls (Fig. 1A) expected from a long history of erosion and soil deposition. The infrared and radar maps similarly show almost no blockiness. The subdued structure of Aratus A, when compared with the sharply defined but equally block-free Hadley C, again suggests an unusual geology for the latter.

It appears that useful geologic information can be drawn from earth-based radar and infrared studies of the lunar surface. The measured quantities are strongly influenced by structure on a scale much finer than the basic instrumental resolution and yet coarse enough to detect the rocks scattered by the events that shaped the present surface. We hope that the information returned from the Apollo 15 mission will be of such a nature that we can check the conclusions in this report; thus, we can either correct our understanding of the data or can proceed with confidence to examine other areas of the lunar surface.

S. H. Zisk
Lunar Science Institute, Houston, Texas 77058, and *Massachusetts Institute of Technology (Haystack Observatory), Westford 01886*

M. H. Carr
Lunar Science Institute and *U.S. Geological Survey, Menlo Park, California 94025*

H. Masursky
Lunar Science Institute and *U.S. Geological Survey, Flagstaff, Arizona 86001*

R. W. Shorthill
Lunar Science Institute and *Boeing Scientific Research Laboratories, Seattle, Washington 98124*

T. W. Thompson
Lunar Science Institute and *Jet Propulsion Laboratory, Pasadena, California 91103*

References and Notes

1. T. W. Thompson, H. Masursky, R. W. Shorthill, S. H. Zisk, G. L. Tyler, *Contrib. 16* (Lunar Science Institute, Houston, Tex., 1970).
2. T. W. Thompson, *Res. Rep. RS73* (Center for Radiophysics and Space Research, Cornell University, Ithaca, N.Y., April 1968).
3. "Final Report/Radar Studies of the Moon," (NASA contract NAS 9-7830, M.I.T. Lincoln Laboratory, Lexington, 28 February 1970).
4. "Polarized" and "depolarized' are defined, respectively, as the sense of circular polarization expected from a plane reflector and the orthogonal sense of polarization.

5. T. W. Thompson, J. B. Pollach, M. J. Campbell, B. T. O'Leary, *Radio Sci.* **5**, 253 (1970); T. Hagfors, *ibid.*, p. 189.
6. M. J. Campbell and J. Ulrichs, *J. Geophys. Res.* **74**, 5867 (1969).
7. R. W. Shorthill, *Spacecr. Rockets* **7**, 385 (1970).
8. E. C. Roelof, *Icarus* **8**, 138 (1968).
9. D. R. Winter, *Radio Sci.* **5**, 229 (1970).
10. R. J. Hackman, *Geologic Map I-463* (LAC 41, U.S. Geological Survey, Washington, D.C., 1966).
11. R. L. Sutton, R. M. Batson, K. B. Larson, J. D. Schafer, R. E. Eggleton, G. A. Swann, *Interagency Rep. 28* (U.S. Geological Survey, Washington, D.C., 1971).
12. On the 3.8-cm radar map (Fig. 1C), Hadley Rille begins as the eastern component of the double bright line at about 25°N, 2.5°E. The western component at that location is the cleft at the southern end of the rille, and the rille continues north past Hadley C.
13. R. Greeley, *Science* **172**, 722 (1971).
14. E. M. Shoemaker, M. H. Hart, G. A. Swann, D. L. Schleicher, G. G. Schaber, R. L. Sutton, D. H. Dahlem, E. N. Goddard, A. C. Waters, *Geochim. Cosmochim. Acta* **3** (Suppl. 1), 2399 (1970).
15. G. P. Kuiper, E. A. Whitaker, R. G. Strom, J. W. Fountain, S. M. Larson, *Consolidated Lunar Atlas* (Contribution 4, Lunar and Planetary Laboratory, University of Arizona, Tucson, 1967), plate C III.
16. Special thanks to H. J. Moore for helpful comments and discussions. This study was sponsored by the Lunar Science Institute under the joint support of the Universities Space Research Association and the NASA Manned Spacecraft Center under contract NSR 09-051-001. Work at Haystack Observatory was supported by NASA Manned Spacecraft Center under contract NAS 9-7830. Work at Jet Propulsion Laboratory was supported by NASA under contract NAS 7-100. Contribution 76, Lunar Science Institute, Houston, Tex.

23 June 1971

Jupiter: Its Captured Satellites

Abstract. *Because of the small size and irregular orbits of the seven outer satellites of Jupiter, it is often assumed that they were derived by capture. The conditions whereby Jupiter can capture satellites have therefore been examined. Relationships derived on the basis of the three-body problem for planets in elliptical orbits enable the dimensions of the capture orbits around Jupiter to be calculated. It is found that Jupiter may capture satellites through the inner Lagrangian point when at perihelion or at aphelion. Captures at perihelion should give rise to satellites in direct orbits of* 11.48×10^6 *kilometers and capture at aphelion to retrograde orbits of* 21.7×10^6 *kilometers. The correspondence with the seven outer satellites suggests that Jupiter VI, VII, and X in direct orbits at 11.47, 11.74, and* 11.85×10^6 *kilometers were captured at Jupiter perihelion, whereas Jupiter VIII, IX, XI, and XII in retrograde orbits of 23.5, 23.7, 22.5, and* 21.2×10^6 *kilometers were captured when Jupiter was at aphelion. Examination of the precapture orbits indicates that the seven outer satellites were derived from the asteroid belt.*

There appear to be two types of satellites in the solar system. Satellites of the first type are relatively large and have approximately circular orbits in the plane of rotation of the primary with which they are associated, and they were presumably derived from the processes that led to the formation of the planets themselves. Satellites of the second type are usually very small and in irregular orbits of large eccentricity and inclination. The orbits may also be direct or retrograde. It is often assumed that this type of satellite was derived by capture from elsewhere in the solar system.

Satellite capture can be analyzed in the restricted three-body problem for planets in elliptical orbits. Relationships developed in terms only of the mass of the planet relative to that of the sun and the eccentricity of the planetary orbit enable the possibility for capture of satellites by any particular planet to be determined (*1*). It is found that for smaller planets the eccentricity becomes a critical factor determining the possibility of capture.

Satellite capture may occur through the inner Lagrangian point only when the planet is at perihelion or aphelion (*2*). Capture at perihelion usually gives rise to satellites in direct orbits and capture at aphelion usually leads to retrograde orbits. Because of their small masses most of the planets can capture satellites only when at perihelion. This is related to the fact that the relative energy required to pass through the inner Lagrangian point is least when the planet is closest to the sun. Captured satellites of the smaller planets would be expected to be in direct orbits about the primary.

It was found for Jupiter, however, that the mass is sufficiently large so that capture of satellites at aphelion into retrograde orbits is also possible.

The 12 satellites of Jupiter appear to be of two distinct types. The Galilean satellites, Io, Europa, Ganymede, and Callisto, are large, with diameters ranging from about 3000 to 5000 km; they are in circular orbits of essentially zero inclination at distances ranging up to 1.88×10^6 km from the planet (*3*).

The seven outer satellites, Jupiter VI through XII, are small, however, with diameters ranging in size from about 12 to 100 km; they are in highly inclined and eccentric orbits at distances up to 23.7×10^6 km from Jupiter. In addition, four of these outer satellites are in retrograde orbits.

The relationships developed for purposes of examining satellite capture have been developed further and are applied here to calculation of the expected dimensions of the direct and retrograde capture orbits about Jupiter.

The Jacobian constant C in the circular, restricted three-body problem may be expressed as

$$C = 2\Omega - V^2$$

Table 1. Orbital parameters of the satellites of Jupiter and predicted capture orbits. Orbital parameters and diameters are from Allen (*3*). The dimensions of the capture orbits were calculated from Eqs. 2 and 3 of this report. In the fourth column, R denotes a retrograde satellite.

Satellite	Diameter (km)	Eccentricity	Inclination (deg)	Distance from planet ($km \times 10^6$)	
				Observed	Calculated for capture orbit
I (Io)	3340	0	0	0.42	
II (Europa)	2920	0	0	0.67	
III (Ganymede)	5700	0	0	1.07	
IV (Callisto)	4720	0	0	1.88	
V	140	0	0.4	0.18	
VI	100	0.16	28	11.47	
VII	20	0.21	26	11.74	11.48*
X	14	0.14	29	11.85	
VIII	20	0.40	33 R	23.5	
IX	16	0.27	25 R	23.7	
XI	16	0.21	17 R	22.5	21.7†
XII	12	0.16	33 R	21.2	

* Direct orbits. † Retrograde orbits.